ChemComm

Check for updates

Flexible, shape-editable wood-based functional materials with acetal linkages†

Yi Tan, [ac] Kaili Wang, [b] Shanshan Gong, [a] Hui Chen, [a] Youming Dong, [b] Qiang Gao, [a] Chengguo Liu *[c] and Jianzhang Li *[a]

A flexible, shape-editable transparent wood (ATW) composite containing acetal linkages was prepared simultaneously through free radical polymerization and addition reaction between vinyl ether bonds and hydroxyl groups. In this system, the anisotropic hierarchical structure of wood acted as a reinforced skeleton, the flexible chain segment ensured flexibility at room temperature, and the dynamic acetal bonds were responsible for the shape memory and editability under relatively mild conditions, verifying the expanding applications of functionalized wood-based materials.

Considering global plastic production exceeds 400 million tons per year,[1] added-value bio-composites have attracted major attention due to the advantageous integrations including biomass raw material and functional design feasibility,[2] which have exhibited the potential to realize multi-functions including transparency, high strength, and thermal insulation, *etc.* Currently, the development of functionalized wood-based materials has become one of the ways to implement carbon-neutral strategies, and the research on transparent wood (TW) aiming at high-value utilization has attracted much attention.[3] The fabrication of TW uses a composite design utilizing a top–down delignified hierarchical structure and refractive index-matched matrix, such as methyl methacrylate, epoxy resin, and styrene.[4–6] The TW composites exhibit anisotropy, transparency, and mechanical performance, and can be applied as building,[7] photonic,[8] and optoelectrical materials.[3] However, the

obtained TWs are usually rigid and cannot be shaped or re-edited,[7,9] which exerts negative impacts on the exploration of the TWs for on-demand functional applications.

Dynamic covalent polymers possess both thermo-plasticity and thermosetting properties,[10] with dynamic covalent networks (DCNs) maintaining mechanical strength and dynamic behavior,[11] and showing shape memorability and editability. Therefore, DCNs possessing matched refractive index with cellulose are expected to be ideal candidates for the preparation of shape-editable TW. Existing studies have shown that the DCN-containing wood composites exhibited high stiffness, and required higher temperature to realize the shape transformation and editing,[12,13] which were not suitable for application scenarios under mild conditions. Therefore, further development of DCN-containing wood composites with flexibility at room temperature is beneficial to promote the functionalization applications. Fortunately, acetal linkage has demonstrated excellent re-processability, is catalyst-free and the response temperature could be regulated after optimization.[14]

In this study, a flexible and shape-editable transparent wood (ATW) composite was constructed *via* addition reaction of the vinyl ether bond with hydroxyl groups forming acetal linkage and free radical polymerization (Fig. 1(a) and (b)). With the hierarchical structure of the delignified wood skeleton (WS) guaranteeing the mechanical properties, the resultant ATW demonstrated good thermal insulation and stability, and ideal optical transmittance and haze. Meanwhile, the shape memorability, editability, and flexibility derived from the lower glass transition temperature (T_g) and dynamic exchange (Fig. 1(c)) are expected to be utilized in flexible material fields, providing a new way for the functionalization of wood-based materials.

Utilizing the WS and acetal-based network (AN) polymer, the ATW with low T_g was constructed by a one-pot radical copolymerization between mixed styrene monomer (SM), 2-ethylhexyl methacrylate (EMA) and hydroxyethyl methacrylate (HEMA) and the addition reaction of hydroxyl and vinyl ether groups (Fig. 1(a)). The system was established to use delignified wood as the reinforced skeleton, 1,4-cyclohexanedimethanol divinyl ether (CDE) as the source of vinyl ether bonds, HEMA as the source of

a State Key Laboratory of Efficient Production of Forest Resources, MOE Key Laboratory of Wooden Material Science and Application, Beijing Key Laboratory of Wood Science and Engineering, Beijing Forestry University, Beijing 100083, China

b Co-Innovation Center of Efficient Processing and Utilization of Forest Resources, College of Materials Science and Engineering, Nanjing Forestry University, 159 Longpan Road, Xuanwu District, Nanjing, 210037, China

c College of Chemical Engineering, Nanjing Forestry University, 159 Longpan Road, Xuanwu District, Nanjing, 210037, China

† Electronic supplementary information (ESI) available: Experimental section, photograph and SEM images of NW and WS, FTIR spectrum and XPS spectra, optical performance of T-ATW, mechanical performances of AN and samples, thermal conductivity and TG and DTG curves of AN, shape recovery properties of ATW and edited ATW, comparison table of the multi-aspect performances of wood composite. See DOI: https://doi.org/10.1039/d4cc03522d
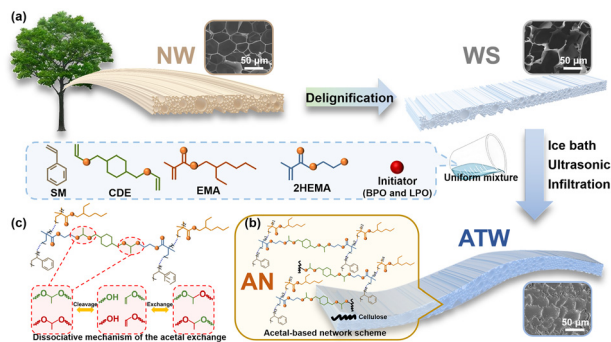
Fig. 1 Schematic illustration of (a) preparation, (b) bonding mechanism of ATW and (c) dissociative mechanism of AN.

hydroxyl groups, SM and EMA as the comonomers to modulate the flexibility of the cross-linked network, benzoyl peroxide (BPO) and lauroyl peroxide (LPO) as free radical initiators, and octadecyl acrylate (OA) for eliminating bubbles.

The light brown native wood (NW) exhibited a multi-scale hierarchical and anisotropic porous structure,[15] with light absorbance and scattering effect (Fig. S1a, ESI†). However, after removing the chromophores in lignin, the WS turned white with loosened cell walls and the inherited hierarchical structure (Fig. S1b, ESI†), and the density was reduced to 0.08 g cm^{-3} (Fig. 2(a)), with lignin content decreased (Fig. 2(b)).[16] The Fourier transform infrared (FTIR) spectra (Fig. 2(c) and Fig. S2a, ESI†) demonstrated the chlorination reaction through the intensity variation of absorption peaks attributed to the aromatic vibrations in lignin,[17] uronic acid groups of the hemicellulose or the ester linkage of the carboxyl groups of lignin and hemicellulose, and carboxyl groups in hemicellulose (xylan/glucomannan).[18,19]

Based on the WS porous structure, the AN polymers were introduced into the composite system to fill the microchannels and holes sufficiently. The AN precursor was prepared by

mixing the vinyl ether source (CDE), comonomers (SM, EMA and HEMA), initiators, and defoaming agent. The free radical copolymerization and addition reaction were confirmed in Fig. S2b (ESI†). The disappearance of the absorption peaks of O–H stretching vibrations (around 3400 cm^{-1}) from HEMA and C=C groups from CDE (1660–1630 cm^{-1}) indicated that the cross-linked network was successfully formed,[14,20,21] as well as the existence of the C=O groups absorption in AN (1721 cm^{-1}), and the density of the cured AN was 1.09 g cm^{-3} (Fig. 2(a)). The free radical polymerization reaction was completed by SM, HEMA and EMA, and the addition reaction occurred between the hydroxyl and vinyl ether groups.[14,22] The ATW displayed a FTIR spectrum (Fig. 2(c)) combining the characteristics of WS and AN, in which the peak shift for the hydroxyl groups indicated the strong interactions between WS and AN,[23] and the density of ATW was reduced to 0.95 g cm^{-3} attributed to the introduction of light weight WS (Fig. 2(a)). The ATW showed a hierarchical porous structure filled with AN (Fig. 2(d)), and the tight integration and interfacial combination revealed in the CT tomoscan image facilitated the reduction of the scattering effect with interfacial pores smaller than 10 μm (Fig. 2(e)), resulting in the transparency of the composite. Additionally, the X-ray photoelectron spectroscopy (XPS) and ^{13}C NMR analysis (Fig. S2c and d, ESI†) manifested the acetal bonds formation and combination mechanism, with the acetal groups' peak appearing and several peaks shifting. The related XPS peaks of ATW and AN are listed in Table S1 (ESI†).[20,24,25]

As shown in Fig. 3(a), the refractive index of AN at 800 nm was 1.44, which approached that of cellulose (1.53),[3] and the AN exhibited a transmittance of 84.40% at 800 nm in Fig. 3(b). Thanks to the matching refractive indices of cellulose and AN, the ATW exhibited a transparent appearance (longitudinal 78.74% transmittance at 800 nm, Fig. 3(b)), which could be applied in light management. Additionally, the ATW possessed ultraviolet (UV) absorption ability due to the existence of the benzene ring and other aromatic ring structures as well as the residual phenylpropane and phenolic hydroxyl groups in WS,[26] which could protect indoor environments from solar UV radiation. Meanwhile, the light scattering at the ATW interfaces
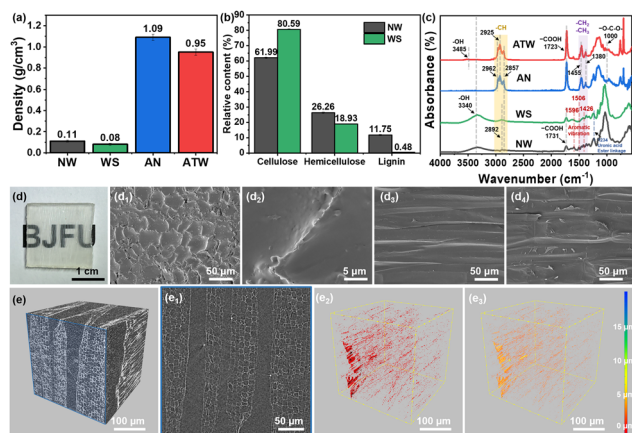

Fig. 2 (a) Density of NW, WS, AN and ATW. (b) Composition contents of cellulose, hemicellulose and lignin for NW and WS. (c) FTIR spectra of NW, WS, AN and ATW. (d) Photograph of ATW: (d$_1$)–(d$_4$) transverse (two magnifications), radial, and tangential SEM images of ATW. (e) The μ-CT tomoscan images: (e$_1$) the cross section of ATW; (e$_2$) and (e$_3$) the interfacial porosity distribution in ATW.

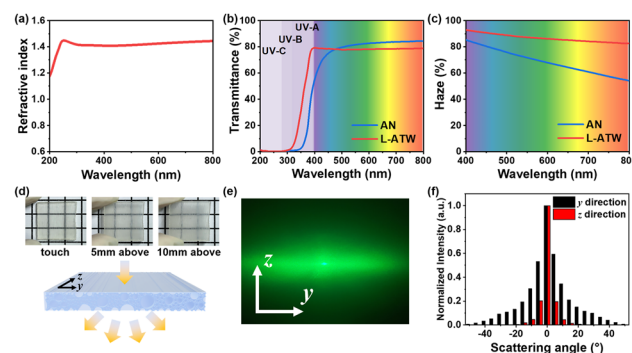**Fig. 3** (a) Refractive index of AN. (b) and (c) Total transmittance and haze of ATW and AN (thickness = 2 mm). (d) Digital images of ATW above the checkerboard pattern. (e) Photograph of the distribution of scattered light spots for ATW. (f) Normalized scattered light intensity distribution for ATW.

resulted in the high haze property (82.63% at 800 nm, Fig. 3(c)), which could overcome the glaring problem of AN with high transmittance and low haze (54.07% haze at 800 nm, Fig. 3(c)). The high haze of ATW could be utilized for protecting internal privacy, providing a consistent and uniform indoor illumination, and the improved light capturing ability could increase the discharge power output in light regulation and energy storage systems.[27]

Furthermore, the optical effect of ATW varied slightly with different distances above the grid pattern (Fig. 3(d)), which was derived from the discrete index variation in the y direction within the oriented WS (Fig. 3(e)), and the image of longitudinal ATW (L-ATW) at a distance of 10 mm above the pattern was clearer than previous studies,[16,28] demonstrating the desired transparency and imaging effect. The discrete index variation resulted in an elliptic spot in which the light intensity along the y direction was obviously stronger, facilitating light-guiding and avoiding light pollution.[29] Meanwhile, the anisotropy of WS endowed transverse ATW (T-ATW) with a different light propagation state (Fig. S3, ESI†), where the light distribution appeared like a radial circle due to the homogeneous structure of cellulose along two directions (Fig. S4, ESI†), and the transmittance and haze were 76.57% and 94.58%, respectively (Fig. S5, ESI†). The unique anisotropic imaging effect, benign transparency and haze endowed the ATW with the potential to act as an optical management material that could be used in energy-efficient buildings, decorative materials, and optoelectronic devices.[16]

Moreover, the ATW demonstrated improved mechanical performance. In Fig. 4(a), the tensile strength of L-ATW reached 13.91 MPa, which was obviously higher than that of longitudinal NW, namely L-NW, (5.11 MPa) and longitudinal WS, namely L-WS, (4.09 MPa), and the fracture strain of L-ATW dramatically increased to 9.74%, which outclassed that of L-NW (1.57%) and L-WS (1.34%). Meanwhile, the tensile strength of T-ATW was 6.47 MPa, which was approximately 6 and 12 times the tensile strengths of transverse NW, *i.e.* T-NW, (1.06 MPa) and transverse WS, *i.e.* T-WS, (0.54 MPa), respectively. The tensile strength of AN was 0.86 MPa (Fig. S6, ESI†), with a high fracture strain of 609.75% indicating the superior flexibility, and the strength discrepancy between ATW and AN manifested

that the compact combination of AN and WS could guarantee the desirable strength of ATW. In the aspect of flexural strength, the AN was too flexible to obtain a characterization result (Table S2, ESI†). The L-ATW (23.62 MPa) exhibited higher flexural strength than L-NW (17.51 MPa) and L-WS (12.22 MPa), while the flexural strength of T-ATW was 6.70 MPa, obviously higher than that of T-NW (1.79 MPa). The results indicated the synergistic effect of the inherited hierarchical structure and benign interfacial combination, as well as the dynamic hydrogen bond interactions,[30] which can be attributed to the mechanism of crack deflection, interfacial delamination, crack branching, and crack bridging within the system.[16]

As a dynamic polymer, the AN with dynamic acetal bond linkages was supposed to feature two characteristic temperatures, the T_g and the topological transition temperature (T_v).[31] As depicted in Fig. 4(e) and (f), the DSC curve indicated the T_g of AN was 20.23 °C, and the dilatometry experiment exhibited a T_g of 19.06 °C and a T_v of 80.02 °C. The relatively lower T_g maintained the flexibility of ATW when exposed to mild temperature, exhibiting superiority over most existing DCNs.[32,33] When the temperature was lower than 20 °C, the unmovable molecular chains and chain segments were in a glassy state. When the temperature was raised to 20–80 °C, the internal molecular chain segment could be transformed into an active state, and the overall polymer was highly elastic.[32] When the temperature was further increased to above 80 °C, the internal molecular chain and chain segment became movable, and the internal acetal bonds could exchange, realizing the reversible dynamic exchange, leading to the rearrangement of the topology structure within the AN.[33] Fig. S7a (ESI†) reveals the rearrangement mechanism of the dynamic exchange of acetal bonds, including the metathesis of acetal and trans-acetalization simultaneously,[34] which can lead to the rearrangement of the molecular topology to realize the morphology deformation, enabling the shape editing.[35]

The thermal conductivity of ATW was 0.22 W m^{-1} K^{-1} (Fig. S7b, ESI†), about one fifth of that of commercial glass,[7] and the lower thermal conductivity can be attributed to the introduction of heat-insulating WS, illustrating that the fabricated ATW could reduce unnecessary heat dissipation and promote energy saving.[36] Furthermore, the TGA characterization results in Fig. S7c and d† indicated there was no obvious mass loss in ATW until 200 °C, manifesting the good thermal stability.

Benefiting from the thermosetting characteristics and thermo-plasticity of DCNs, ATW underwent shape recovery and editing under thermal stimulation. As shown in Fig. 5(a), ATW could undergo various shape changes under 40 °C with activated molecular chains, changing from a flat strip to a U shape after cooling for fixing, and then ATW could gradually recover to a flat strip shape under reheating with molecular chains returned to the lowest energy configuration.[37] As shown in Fig. 5(b), ATW could recover to 91.61° within 3 min and 173.82° within 25 min, with a recovery rate of about 96.57% (Fig. S8, ESI†). In addition, the shape memory effect of ATW had desirable stability, and the recovery rate over 10 cycles was maintained at more than 95% (Fig. S8 (c)). The exchange mechanism of acetal bonds in AN involved the metathesis of acetal
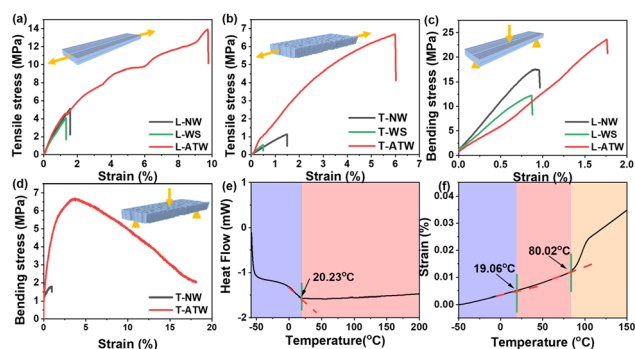
Fig. 4 (a) and (c) Tensile and three-point bending stress−strain curves of L-NW, L-WS, and L-ATW. (b) and (d) Tensile and three-point bending stress−strain curves of T-NW and T-ATW. (e) and (f) DSC and dilatometry experiment curves of AN.
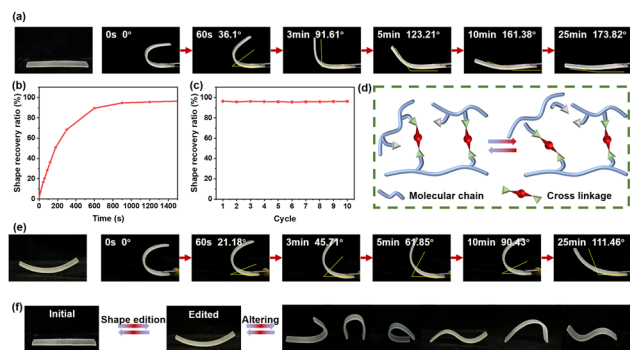
Fig. 5 (a) Shape recovery photographs of ATW at different time points. (b) Shape recovery curve of ATW at 40 °C. (c) Shape recovery ratio of ATW over 10 cycles at 40 °C. (d) Shape editing mechanism. (e) Shape recovery photographs of edited ATW. (f) Shape editing and altering of edited ATW.

and trans-acetalization simultaneously, which could guarantee the shape editing of ATW (Fig. 5(d)).[34] As shown in Fig. 5(e), the flat strip ATW was edited and fixed for 10 min at 80 °C under a small external force, followed by cooling. The edited ATW could still be transformed into different shapes (Fig. 5(f)), showing shape memorability with an outstanding recovery effect under relatively mild conditions (Fig. S9, ESI†). Therefore, the resultant ATW exhibited obvious shape memorability and editability.

In summary, a flexible, shape-editable transparent wood (ATW) was prepared by forming acetal linkage between vinyl ether bonds and hydroxyl groups and free radical polymerization. Benefiting from the match of refractive indices and tight combination between the low-T_g AN matrix and WS, the dynamic behavior of the acetal bonds under mild conditions, and the anisotropic hierarchical structure of WS, the fabricated ATW exhibited flexibility, obvious optical transparency, UV isolation, heat insulation, excellent mechanical properties, shape memorability, and editability. Furthermore, it possessed comprehensive advantages in visual effects, mechanical properties, and response temperatures, which can promote expansion of applications of wood-based composites.

Data availability

The data supporting this article have been included as part of the supplementary information.†

Conflicts of interest

There are no conflicts to declare.

Notes and references

1 W. Cowger, K. A. Willis, S. Bullock, K. Conlon, J. Emmanuel, L. M. Erdle, M. Eriksen, T. A. Farrelly, B. D. Hardesty, K. Kerge, N. Li, Y. Li, A. Liebman, N. Tangri, M. Thiel, P. V. Gómez, T. R. Walker and M. Wang, *Sci. Adv.*, 2024, **10**, eadj8275.
2 A. K. Mohanty, S. Vivekanandhan, J. Pin and M. Misra, *Science*, 2018, **362**, 536–542.
3 S. Zhu, S. Kumar Biswas, Z. Qiu, Y. Yue, Q. Fu, F. Jiang and J. Han, *Prog. Mater. Sci.*, 2023, **132**, 101025.
4 T. Keplinger, F. K. Wittel, M. Ruggeberg and I. Burgert, *Adv. Mater.*, 2021, **33**, e2001375.
5 M. Zhu, J. Song, T. Li, A. Gong, Y. Wang, J. Dai, Y. Yao, W. Luo, D. Henderson and L. Hu, *Adv. Mater.*, 2016, **28**, 5181–5187.
6 X. Wu, Z. Kong, X. Yao, J. Gan, X. Zhan and Y. Wu, *Appl. Surf. Sci.*, 2023, **613**, 155927.
7 R. Mi, T. Li, D. Dalgo, C. Chen, Y. Kuang, S. He, X. Zhao, W. Xie, W. Gan, J. Zhu, J. Srebric, R. Yang and L. Hu, *Adv. Funct. Mater.*, 2020, **30**, 1907511.
8 Y. Li, E. Vasileva, I. Sychugov, S. Popov and L. Berglund, *Adv. Opt. Mater.*, 2018, **6**, 1800059.
9 K. Wang, Y. Dong, Z. Ling, X. Liu, S. Q. Shi and J. Li, *Compos. Sci. Technol.*, 2021, **207**, 108690.
10 W. Liu, S. Yang, L. Huang, J. Xu and N. Zhao, *Chem. Commun.*, 2022, **58**, 12399–12417.
11 L. You, *Chem. Commun.*, 2023, **59**, 12943–12958.
12 C. Xiong, B. Li, H. Liu, W. Zhao, C. Duan, H. Wu and Y. Ni, *J. Mater. Chem. A*, 2020, **8**, 10898–10908.
13 K. Wang, T. Zhang, C. Li, X. Xiao, Y. Tang, X. Fang, H. Peng, X. Liu, Y. Dong, Y. Cai, D. Tian, Y. Li and J. Li, *Composites, Part B*, 2022, **246**, 110260.
14 N. Lu, Q. Li, S. Ma, B. Wang, X. Xu, S. Wang, J. Ye, J. Qiu and J. Zhu, *Eur. Polym. J.*, 2021, **147**, 110291.
15 S. Wei, C. Wan, Y. Jiao, X. Li, J. Li and Y. Wu, *Chem. Commun.*, 2020, **56**, 340–343.
16 Y. Tan, K. Wang, Y. Dong, S. Gong, S. Q. Shi and J. Li, *Chem. Eng. J.*, 2022, **448**, 137487.
17 Q. Xia, C. Chen, T. Li, S. He, J. Gao, X. Wang and L. Hu, *Sci. Adv.*, 2021, **7**, eabd7342.
18 W. Gan, S. Xiao, L. Gao, R. Gao, J. Li and X. Zhan, *ACS Sustainable Chem. Eng.*, 2017, **5**, 3855–3862.
19 Z. Jiang, J. Yi, J. Li, T. He and C. Hu, *ChemSusChem*, 2015, **8**, 1901–1907.
20 T. Wang, L. Li, Q. Wang, G. Xie and C. Guo, *Ind. Crops Prod.*, 2019, **141**, 111798.
21 Z. P. Zhang, M. Z. Rong and M. Q. Zhang, *Adv. Funct. Mater.*, 2018, **28**, 1706050.
22 Q. Li, S. Ma, S. Wang, Y. Liu, M. A. Taher, B. Wang, K. Huang, X. Xu, Y. Han and J. Zhu, *Macromolecules*, 2020, **53**, 1474–1485.
23 L. Cheng and J. Feng, *Composites, Part A*, 2020, **129**, 105690.
24 L. Breloy, C. A. Ouarabi, A. Brosseau, P. Dubot, V. Brezova, S. Abbad Andaloussi, J. P. Malval and D. L. Versace, *ACS Sustainable Chem. Eng.*, 2019, **7**, 19591–19604.
25 S. Chen, L. Chen, Y. Wang, C. Wang, M. Miao and D. Zhang, *Eur. Polym. J.*, 2019, **120**, 109254.
26 F. Zou, H. Li, Y. Dong, G. C. Tewari and J. Vapaavuori, *Chem. Eng. J.*, 2022, **439**, 135738.
27 R. F. Beims, R. Arredondo, D. J. Sosa Carrero, Z. Yuan, H. Li, H. Shui, Y. Zhang, M. Leitch and C. C. Xu, *Renewable Sustainable Energy Rev.*, 2022, **157**, 112074.
28 Y. Tan, K. Wang, Y. Dong, S. Gong, Y. Lu, S. Q. Shi and J. Li, *ACS Nano*, 2024, **18**, 6718–6730.
29 J. Wu, Y. Liang, C. Xia, X. Ma, B. Fei, Y. Wu, S. Ge, J. Lu, J. Li and Z. Xia, *Adv. Mater. Technol.*, 2023, **8**, 2200704.
30 M. Mottoul, S. Giljean, M. J. Pac, V. Landry and J. F. Morin, *J. Appl. Polym. Sci.*, 2023, **140**, e53853.
31 N. J. Van Zee and R. Nicolaÿ, *Prog. Polym. Sci.*, 2020, **104**, 101233.
32 J. Luo, Z. Demchuk, X. Zhao, T. Saito, M. Tian, A. P. Sokolov and P. Cao, *Matter*, 2022, **5**, 1391–1422.
33 B. Krishnakumar, R. V. S. P. Sanka, W. H. Binder, V. Parthasarthy, S. Rana and N. Karak, *Chem. Eng. J.*, 2020, **385**, 123820.
34 Q. Li, S. Ma, S. Wang, W. Yuan, X. Xu, B. Wang, K. Huang and J. Zhu, *J. Mater. Chem. A*, 2019, **7**, 18039–18049.
35 S. Grauzeliene, M. Kastanauskas, V. Talacka and J. Ostrauskaite, *ACS Appl. Polym. Mater.*, 2022, **4**, 6103–6110.
36 R. Mi, C. Chen, T. Keplinger, Y. Pei, S. He, D. Liu, J. Li, J. Dai, E. Hitz, B. Yang, I. Burgert and L. Hu, *Nat. Commun.*, 2020, **11**, 3836.
37 C. Huang, J. Peng, Y. Cheng, Q. Zhao, Y. Du, S. Dou, A. P. Tomsia, H. D. Wagner, L. Jiang and Q. Cheng, *J. Mater. Chem. A*, 2019, **7**, 2787–2794.